Thermopervaporation for regeneration of triethylene glycol (TEG):Experimental and model development

Kristin Dalane, Natalie Therese Josefsen, Luca Ansaloni, Magne Hillestad**, Liyuan Deng*

Department of Chemical Engineering, Norwegian University of Science and Technology (NTNU), Sem Sælandsvei 4, N-7491, Trondehim, Norway

ABSTRACT

Subsea processing is getting increased interest in the oil and gas sector as it can provide broader exploration of the oil and gas with a lower environmental footprint. Dehydration of natural gas with the use of triethylene glycol (TEG) is one of the main processing step for natural gas treatment to avoid transportation problems caused by the presence of water. Distillation is a commonly used technology for topside regeneration of TEG. However, for subsea operation alternative technologies are required to avoid complexity and the large energy consumption. Membranes are evaluated as promising solutions as they fulfil the subsea design criteria of compact design, flexible operation, and high modularity. In this work, the use of thermopervaporation for regeneration of TEG has been assessed. A mathematical model of a plate-and-frame thermopervaporation membrane module has been developed, where two-dimensional flow are considered for the liquid phases and the air gap is treated as a stagnant phase. Experimental pervaporation data were provided for the tuning of the model and the development of a temperature dependent permeability correlation. In addition, the effects of operation conditions and membrane properties on the separation performance were investigated. From this evaluation, it is clearly shown that the air gap significantly affects the separation performance and is a key parameter in the design of the thermopervaporation module.

1. Introduction

Subsea processing technology is considered as an enabling technology for production from more difficult fields located at larger water depths, longer tie-back distances and in colder/harsher environments [1]. Compared to the other fossil fuels, natural gas is an environmental friendly clean fuel. To ensure safe processing and transmission of the natural gas the water content in the gas from the reservoir needs to be reduced and controlled [2]. Natural gas dehydration can be achieved through different methods, such as solid adsorption or liquid absorption [3]. Nowadays, the most commonly used technology in the oil and gas industry is absorption using glycols, where triethylene glycol (TEG) is the most used [4]. The common technology for topside regeneration is distillation, but its system complexity and the large energy consumption fosters the research for alternative technologies for subsea operation [5]. Compact design, high modularity, and flexible operation make membrane pervaporation a promising solution [6]. Natural gas dehydration using a closed-loop membrane process has been reported in our prior work [6], which includes a membrane contactor operating at high pressure to dehydrate the natural gas and a thermopervaporation unit

to regenerate the H_2O-rich glycol absorbent. In a previous work [7], the developed model for the membrane contactor for dehydration of natural gas with TEG has been reported.

Pervaporation combines the permeation through a membrane and evaporation, possibly leading to higher recovery of the absorbent. This combination results in pervaporation being considered as a cost-effective technology as mainly the minor component is involved in the evaporation and the separation efficiency is increased due to the use of a selective membrane [8]. Three different process configurations can be used to achieve a low vapour pressure on the permeate side and hence maximize the driving force. The operation configurations are the use of a sweep gas, or a vacuum pump, or alternatively by condensation (normally called thermopervaporation) [8–10]. The use of vacuum is the most common method in experimental studies and commercial use. Despite for the large potential of pervaporation in different application, the main industrial application is dehydration of organic solvents, especially dehydration of ethanol [11]. Wijmans et al. [12] have patented the use of pervaporation for regeneration of TEG in combination with a conventional contacting tower for dehydration of the natural gas. For subsea operation, the use of a vacuum pump or sweep gas are

---

less feasible, and thermopervaporation could be a promising technology due to the unlimited amount of cooling water from the sea.

Several researchers [13–21] have investigated glycol dehydration using vacuum pervaporation with different types of membranes, but literature data mainly focus on dehydration of monoethylene glycol (MEG) and only one experimental value is available for dehydration of TEG [18]. Due to the different properties of the two glycols, MEG data cannot be considered representative for TEG dehydration. However, in view of the lower volatility compared to MEG, higher separation factor is expected. To the best of authors' knowledge, thermopervaporation has also received little attention in the open literature [22–25], and no data related to glycols are currently available. Therefore, the proper evaluation of the pervaporation potential by means of process simulation is limited by the lack of experimental data. In this view, the present paper provides a systematic study of membrane performance for TEG/ H_2O binary mixtures, aiming at providing a necessary dataset for model implementation. In order to meet the subsea requirements in terms of long-term stability, thin composite membranes (dense coating supported on a porous layer) have been identified as a preferable configuration, as the dense coating is able to prevent issues such as pore wetting, which can seriously hinder the membrane capacity. Therefore, a compatibility test of different membrane materials has been performed, with the scope of identifying a suitable polymer candidate as dense layer coating. Upon the identification of the dense layer materials, thin composite membranes have been prepared and their morphology has been investigated by SEM imaging. Subsequently, pervaporation tests have been performed for pure water and H_2O/TEG mixture (water content up to 30 wt%) in a temperature range between 30 and 50°C. The permeate composition has been detected by gas chromatograph (GC) analysis to identify the separation factor achieved by the pervaporation process.

Based on the experimental data, a permeability correlation required for the implementation of a thermopervaporation model has been developed. To the best of the authors' knowledge, thermopervaporation modelling has received little attention in literature [26,27], and no studies have been found on the investigation of this technology within the dehydration of glycols. From a modelling point of view, air gap membrane distillation and thermopervaporation are similar processes. Therefore, models developed for air gap membrane distillation can be considered of interest for the development of a thermopervaporation model. The main difference lies in the dense coating layer typically used in the membrane configuration for thermopervaporation to improve the process selectivity. Even though additional literature references about membrane distillation modelling [28–32] are found, none of them deals with TEG dehydration. More research was conducted on pervaporation with vacuum operation, and hence more models pervaporation were reported. Even though many of the reported models are focus on describing the membrane flux, some models also describe the membrane modules, which are required for process design and optimization. The reported models cover different pervaporation applications with different module configurations (spiral wound, flat sheet and hollow fiber) and model complexity [33–37].

Thermopervaporation has been evaluated as a potential technology for regeneration of triethylene glycol in a subsea natural gas dehydration system [6]. A model to document feasibility and operation performance is then needed. In this paper, a mathematical model of the thermopervaporation module is developed in MATLAB and solved with the use of orthogonal collocation. In addition, the effects of different membrane module parameters and operation conditions on the separation performance are evaluated.

2. Model development

The thermopervaporation model reported in this paper is based on the plate-and-frame configuration as illustrated in Fig. 1a. The model evaluates one feed channel with the surrounding air gap and one

channel for cooling water, assuming equal performance of all the channels. Steady state is assumed, giving that the amount of H_2O transported over the membrane is equal to the amount condensed in the air gap on the cooling wall. In addition, the liquid condensate is assumed to have equal temperature as the cooling water. The model is a 2D model for the liquid phases, to include temperature profile and for the liquid TEG also the concentration profile in the channel in x-direction. Uniform conditions are considered in y-direction. The mass and energy transport over the membrane to the cooling wall is based on the mass transfer resistance in series model, from the membrane-liquid interface to the cooling wall where the air gap is considered as a stagnant phase. A schematic illustration of the thermopervaporation model is given in Fig. 1b.

2.1. Assumptions

The developed model comprises a set of assumptions as listed below.

1 Steady state
2 Equal performance of each channel
3 Laminar flow for TEG flow and cooling water
4 Equilibrium at gas-liquid interface for the membrane and the cooling wall
5 Uniform conditions in y-direction
6 Liquid condensed from the air gap has equal temperature as the cooling water
7 No liquid film formation of the permeate is considered on the cooling wall

2.2. Velocity profile

Based on the Reynolds number of the liquid flow in the feed channel and cooling water channel, laminar flow is assumed. The axial flow velocity as function of the channel position (x) can be derived as given in Eq. (1). Assuming a parabolic velocity profile implies zero velocity of the liquid at the channel walls, which for a membrane process might not be true due to the mass flux over the membrane. However, it is assumed that a parabolic velocity profile can be used as the flux over the membrane is small compared to the liquid flow in axial direction.

$$v_z = \frac{3}{2} v_{z,av} \left(1 - \left(\frac{x}{\frac{\delta_f}{2}} \right)^2 \right)$$

(1)

where $v_{z,av}$ is the average liquid velocity [m/s], which is the total flow rate divided by the flow cross sectional area, x is the position in x-direction and δ_f is the thickness of the feed channel [m].

2.3. Feed channels

The differential equation for the concentration changes along the membrane module is given by Eq. (2). The liquid phase is modelled as two-dimensional flows, including diffusion in x-direction in addition to the axial convective flow (z-direction), with the assumption of uniform condition in y-direction. With a two-dimensional model, no mass transfer coefficient is needed to include the mass transfer resistance in the liquid boundary layer.

$$v_z \frac{\partial C_{l,i}}{\partial z} = \frac{\partial}{\partial x} \left(D_{l,i} \frac{\partial C_{l,i}}{\partial x} \right)$$

(2)

$C_{l,i}$ is the molar concentration of component i in the liquid phase [kmol/ m^3], x is the x-direction length segment [m] and $D_{l,i}$ is the diffusivity of component i in TEG [m^2/s].

The boundary conditions for Eq. (2) are given in Eqs. (3)–(5).

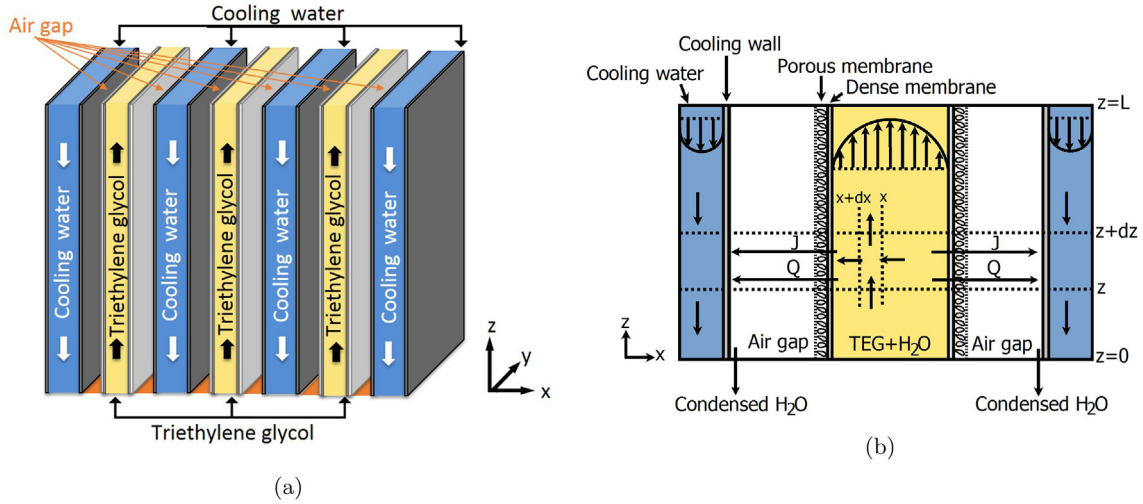$$C_{l,i}(z = 0) = C_{l,i,feed}$$

(3)

Fig. 1. a) Illustration of the plate and frame configuration of the thermopervaporation unit. b) The structure of the thermopervaporation model.

$$\left.\frac{dC_{l,i}}{dx}\right|_{x=0} = 0 \tag{4}$$

$$\left.\frac{dC_{l,i}}{dx}\right|_{x=\frac{\delta_f}{2}} = \frac{-J_i}{D_{l,i}} \tag{5}$$

where $C_{l,i,feed}$ [kmol/m^3] is the feed concentration and J_i is the membrane flux of component i [kmol/m$_m^2$ s].

The temperature changes in the liquid phase are described by the differential equations developed from the energy balance given in Eq. (6), which includes energy flow due to convection and conduction. In z-direction, the heat of conduction is assumed negligible compared to the heat flow by convection.

$$\frac{\partial T_l}{\partial z} = \frac{\lambda_l}{\rho_l C_{p,l} v_z}\frac{\partial^2 T_l}{\partial x^2} \tag{6}$$

T_l is the liquid temperature [K], ρ_l is the liquid phase density [kg/m^3], $C_{p,l}$ is the heat capacity of the liquid phase [J/kg K] and λ_l is the thermal conductivity of the liquid phase [W/m K].

The boundary conditions for Eq. (6) are given in Eqs. (7)–(9).

$$T_l(z=0) = T_{l,feed} \tag{7}$$

$$\left.\frac{dT_l}{dx}\right|_{x=0} = 0 \tag{8}$$

$$\left.\frac{dT_l}{dx}\right|_{x=\frac{\delta_f}{2}} = -\frac{Q}{\lambda_l} - \frac{\Sigma J_i \Delta H_{vap,i}}{\lambda_l} \tag{9}$$

$T_{l,feed}$ is the liquid feed temperature [K], Q is the total heat transfer from the hot liquid to the cooling water [W/m^2], and $\Delta H_{vap,i}$ is the heat of evaporation of component i [J/kmol].

The pressure drop in the feed channel over the membrane length is given in Eq. (10), with the friction factor for laminar flow in a rectangular channel given in Eq. (11) [38].

$$\frac{dP_l}{dz} = f_{D,l}\frac{1}{2}\rho_l v_{z,av}^2 \frac{1}{d_h}\frac{1}{1000} \tag{10}$$

$$f_{D,l} = \frac{96}{Re_l} \tag{11}$$

$$d_h = \frac{2\delta_f L_w}{\delta_f + L_w} \tag{12}$$

where P_l is the liquid phase pressure [kPa], $f_{D,l}$ is the friction factor, Re_l is the feed channel Reynolds number, d_h is the hydraulic diameter of the channel [m] and L_w is the membrane width [m].

2.4. Cooling water channel

The temperature changes in the cooling water channel are the main value of interest for the cooling water. Therefore, a two-dimensional energy balance for the cooling water channel is included in the model using Eq. (13).

$$\frac{\partial T_{cw}}{\partial z} = \frac{-\lambda_{cw}}{\rho_{cw} C_{p,cw} v_{cw}}\frac{\partial^2 T_{cw}}{\partial x^2} \tag{13}$$

T_{cw} is the cooling water temperature [K], ρ_{cw} is the cooling water density [kg/m^3], $C_{p,cw}$ is the heat capacity of the cooling water [J/kg K], v_{cw} is the cooling water velocity [m/s] and λ_{cw} is the thermal conductivity of the cooling water [W/m K].

The boundary conditions for Eq. (13) are given in Eq. (14)–(16).

$$T_{cw}(z=1) = T_{cw,feed} \tag{14}$$

$$\left.\frac{dT_{cw}}{dx}\right|_{x=0} = 0 \tag{15}$$

$$\left.\frac{dT_{cw}}{dx}\right|_{x=\frac{\delta_{cw}}{2}} = -\frac{Q}{\lambda_{cw}} - \frac{\sum J_i \Delta H_{vap,i}}{\lambda_{cw}} \tag{16}$$

$T_{cw,feed}$ is the cooling water feed temperature [K] and δ_{cw} is the thickness of the cooling water channel [m].

2.5. Membrane flux

The flux from the liquid-membrane interface to the condensation in the air gap is found following the resistance in series approach, based on the local driving forces.

$$J_{i,dmem} = \frac{k_{dmem,i}}{R_g T_l}(P_{l,i}^{VLE} - P_{dmem,i}) \tag{17}$$

$$J_{i,pmem} = \frac{k_{pmem,i}}{R_g T_l}(P_{dmem,i} - P_{pmem,i}) \tag{18}$$

$$J_{i,ag} = \frac{k_{ag,i}}{R_g T_{ag,av}}(P_{pmem,i} - P_{ag,i}^{VLE}) \tag{19}$$

$k_{dmem,i}$, $k_{pmem,i}$ and $k_{ag,i}$ are the dense membrane, the porous membrane and the air gap mass transfer resistance coefficients [m/s], R_g is the ideal gas constant [J/mol K] and $T_{ag,av}$ is the average temperature in the air gap [K]. $P_{l,i}^{VLE}$, $P_{dmem,i}$, $P_{dmem,i}$ and $P_{ag,i}^{VLE}$ is the equilibrium partial pressure of component i [kPa] at respectively the liquid-membrane interface, the porous-dense membrane interface, the membrane-air gap

interface and the air gap-condensate interface.

The mass balance and membrane flux equation given above is general equations valid for all components in the system. As H_2O is the main component for flux evaluation in the TEG regeneration process, only H_2O equations are considered in the model. This is supported with experimental results indicating that the TEG content in the permeate is low, below 1000 ppm (see section 3). Eq. (20) gives the overall mass flux from the liquid-membrane interface to the cooling wall in the air-gap for H_2O, under the steady state assumption.

$$J_{H_2O} = \frac{1}{\frac{R_g T_1}{k_{dmem,H_2O}} + \frac{R_g T_1}{k_{pmem,H_2O}} + \frac{R_g T_{ag,av}}{k_{ag,H_2O}}} \left(P_{l,H_2O}^{VLE} - P_{ag,H_2O}^{VLE}\right)$$

(20)

The partial pressure of H_2O on the air gap side at the cooling wall is found equal to the saturation pressure of pure H_2O at the temperature of the condensate, which is assumed equal to the cooling water temperature, by Eq. (21) [39].

$$P_{H_2O,T_{cw}}^{sat} = \exp\left(65.9278 - \frac{7227.53}{T_{cw}} - 7.17695 \ln(T_{cw}) + 4.0313e^{-6}T_{cw}^2\right)$$

(21)

The vapour-liquid equilibrium partial pressure of H_2O over the TEG solution at the membrane liquid interface is found based on the modified Raoult's law, given in Eq. (22). The activity coefficient is included to adapt for non-ideal solution and is calculated based on the model reported by Parrish et al. [40] given in Eq. (23)–(27).

$$P_{l,H_2O}^{VLE} = P_{H_2O,T_{l,mem}}^{sat} \gamma_{H_2O} x_{H_2O}$$

(22)

$$\gamma_{H_2O} = \exp(B(\tanh(\tau_\gamma) - 1)Cx_{TEG}^2)$$

(23)

$$\tau_\gamma = \frac{Ax_{H_2O}}{Bx_{TEG}}$$

(24)

$$A = \exp(-12.792 + 0.03293T_{l,mem})$$

(25)

$$B = \exp(0.77377 - 0.00695T_{l,mem})$$

(26)

$$C = 0.88874 - 0.001915T_{l,mem}$$

(27)

where $T_{l,mem}$ is the temperature of the liquid at membrane interface [K].

The air gap is a stagnant phase for heat and mass transfer and the mass transfer coefficient (k_{ag,H_2O}) is found from the air gap spacing and the diffusivity of H_2O in air given by Eq. (28).

$$\frac{1}{k_{ag,H_2O}} = \frac{\delta_{ag}}{D_{air,H_2O}}$$

(28)

where δ_{ag} is the air gap spacing [m] and D_{air,H_2O} is the diffusivity of H_2O in air [m²/s] which is found with the Fuller et al. correlation [41] at $T_{ag,av}$.

$$D_{air,H_2O} = \frac{0.00143T_{ag,av}^{1.75}}{\frac{P}{100}M_{air,H_2O}^{0.5}[(\Sigma_v)_{air}^{1/3} + (\Sigma_v)_{H_2O}^{1/3}]^2} \frac{1}{10000}$$

(29)

$$M_{air,H_2O} = 2\left[\frac{1}{M_{air}} + \frac{1}{M_{H_2O}}\right]^{-1}$$

(30)

where D_{air,H_2O} is the binary diffusion coefficient [m²/s], $T_{ag,av}$ is the average temperature in the air gap [K], M_{air} and M_{H_2O} is the molecular weight of air and H_2O [g/mol], P is the pressure [kPa] and Σ_v is the sum of atomic diffusion volumes.

Two different diffusion mechanisms can take place in the mass transport over the porous support, namely molecular diffusion and Knudsen diffusion. Molecular diffusion is dominating at pore sizes larger than 0.1 μm and Knudsen diffusion dominates with pore sizes smaller than 50 nm [9]. If both molecular diffusion (D_{air,H_2O}) and Knudsen diffusion (D_{kn,H_2O}) contribute to the mass transport, the porous membrane mass transfer coefficient (k_{pmem}) is given by Eq. (31).

$$\frac{1}{k_{pmem,H_2O}} = \frac{\delta_{mem,p}}{\tilde{D}_{pmem,H_2O}}$$

(31)

$$\frac{1}{\tilde{D}_{pmem,H_2O}} = \frac{\tau_p}{\varepsilon_p}\left(\frac{1}{D_{air,H_2O}} + \frac{1}{D_{kn,H_2O}}\right)$$

(32)

$$\tau_p = \frac{(2 - \varepsilon_p)^2}{\varepsilon_p}$$

(33)

where $\delta_{mem,p}$ is the thickness of the porous membrane [m], τ_p is the tortuosity of the membrane and ε_p is the porosity of the membrane.

The diffusivity coefficient for Knudsen diffusion is found with Eq. (34) [9].

$$D_{kn,H_2O} = \frac{d_p}{3}\sqrt{\frac{8R_g T_l}{\pi \frac{M_{H_2O}}{1000}}}$$

(34)

where d_p is the diameter of the pores [m].

A similar approach as used for the mass transfer can be used for the heat transfer resistance. The total heat flux over the membrane, Q [W/m$_m^2$], is given by Eq. (35), where inner membrane surface is used as transport area basis.

$$Q = \frac{1}{\frac{\delta_{mem,d}}{\lambda_{AF2400}} + \frac{\delta_{mem,p}}{\bar{\lambda}_p} + \frac{\delta_{ag}}{\lambda_{ag}}}(T_{l,mem} - T_{cw})$$

$$= \frac{1}{\frac{\delta_{mem,d}}{\lambda_{AF2400}} + \frac{\delta_{mem,p}}{\frac{(1-\varepsilon_p)\lambda_{PP}}{\tau} + \frac{\varepsilon_p\lambda_{mem,ag}}{\tau}} + \frac{\delta_{ag}}{\lambda_{ag}}}(T_{l,mem} - T_{cw})$$

(35)

λ_{AF2400} and λ_{PP} is the membrane material thermal conductivity [W/m K], $\lambda_{mem,ag}$ and λ_{ag} is the thermal conductivity of air in the membrane pores and the air gap [W/m K] (Eq. (36) and Eq. (37) [42]).

$$\lambda_{mem,ag} = 1.5207 \cdot 10^{-11}T_{l,mem}^3 - 4.8574 \cdot 10^{-8}T_{l,mem}^2 + 1.0184$$
$$\cdot 10^{-4}T_{l,mem} - 3.9333 \cdot 10^{-4}$$

(36)

$$\lambda_{ag} = 1.5207 \cdot 10^{-11}T_{ag,av}^3 - 4.8574 \cdot 10^{-8}T_{ag,av}^2 + 1.0184 \cdot 10^{-4}T_{ag,av} - 3.9333$$
$$\cdot 10^{-4}$$

(37)

2.6. Physical properties

In addition to the mass balance equations, the model also includes correlations for physical properties. Table 1 gives an overview of the main properties correlations, including the functional dependency and the literature source for the correlation.

3. Experimental data and model tuning

Compatibility and pervaporation tests have been performed in order to provide a reliable dataset for the estimation of the thermo-pervaporation potential in regeneration of TEG by water removal. In

Table 1
Physical properties correlations.

Property	Symbol	Function dependence	Source
Diffusivity of H_2O in TEG	D_{l,H_2O}	f(T_l, x_{H_2O})	[41]
Diffusivity of H_2O in air (Molecular diffusion)	D_{air,H_2O}	f(P, T)	[41]
Diffusivity of H_2O in air (Knudsen diffusion)	D_{kn,H_2O}	f(d_p, T_l)	[9]
Heat capacity of TEG	$C_{p,l}$	f(T_l, x_{H_2O})	[43]
Thermal conductivity of TEG	λ_l	f(T_l, x_{H_2O})	[44]
Viscosity of TEG	μ_l	f(T_l, x_{H_2O})	[44]
Density of TEG	ρ_l	f(T_l, x_{H_2O})	[44]
Thermal conductivity of air	λ_{ag}	f(T)	[42]

this context, the data obtained from pervaporation experiments were used to develop a correlation for H_2O permeability through the membrane layer. It is expected that the correlation developed for pervaporation can be used in the thermopervaporation model, as the permeability of the dense layer is an intrinsic property of the membrane material. In addition, the developed model (section 2) accounts for the different boundary conditions, which applies to the different processes.

3.1. Materials and methods

3.1.1. Materials

Several polymeric materials have been investigated to determine their compatibility with TEG. Poly[1-(trimethylsilyl)-1-propyne] (PTMSP) was purchased from Gelest Inc. (Pennsylvania, US); Teflon °AF2400 was purchased from the Chemours Company (Wilmington, US); extruded Nafion membrane (Nafion™ Membrane NR-211) was purchased from Ion Power (Munich, Germany); polydimethylsiloxane (PDMS) was obtained from Sylgard 184 provided by Dow Corning (Lindberg & Lund, Norway); Nexar was provided by Kraton Polymers (Houston, TX). Porous polypropylene Celgard °2400 was kindly supplied by Celgard (Charlotte, NC). 6FDA-Durene polimide and PIM-1 were synthesized according to previous literature [45,46]. FC-72 was purchased from 3 M (Kemi-Intressen, Sweden). Reagent-Plus quality of toluene, cyclohexane, chloroform (CCl4), tetrahydrofuran (THF), triethyelene glycol (TEG) and triethyelene glycol monoethylether (TEG-MEE) was purchased from Sigma Aldrich, and the solvents have been used without further purification.

3.1.2. Membrane preparation

The polymeric samples prepared for the compatibility tests were obtained by solvent casting technique. A calibrated amount of polymer was dissolved in a specific solvent to achieve a solid concentration of 1 wt%, stirred overnight to ensure the achievement of a clear solution and then casted on a petri dish. Upon the solvent evaporation, the membranes were heat treated at a temperature above the boiling point of the solvent under vacuum overnight to ensure a complete solvent removal. The following solvents have been used: cyclohexane in the case of PTMSP, FC-72 in the case of Teflon °AF2400, toluene in the case of PDMS, THF in the case of Nexar, CCl4 in the case of 6FDA-Durene and PIM-1. The prepared samples had a thickness in the range off 50–100 μm.

Upon the identification of the proper polymer candidate, thin composite membranes have been prepared for testing in the pervaporation setup. In particular, thin layers of Teflon °AF2400 were coated on Celgard °2400 (average pore size 43 nm, porosity 41%) by dip-coating technique. 100 ml of 1 wt% solution of Teflon °AF2400 were prepared and dropped in a glass container. The porous support was flattened on a glass plate using aluminium tape to prevent flowing of solution on the back of the support. The glass plate was then dipped inside the casting solution and placed vertically to allow the solvent evaporation. The dipping procedure was repeated twice, flipping the plate of 180° to ensure the homogeneous coating of a defect-free layer of Teflon °AF2400. The thickness of the selective layer was then investigated by SEM imaging. As showed in Fig. S1 (Supplementary material), a coating thickness of about 1.7 μm was achieved.

3.1.3. Membrane characterization

Compatibility of the fabricated membranes was investigated by immersion tests [47] in TEG. The weight of the immersed sample was monitored over time in order to determine the TEG uptake (Ω_{TEG}), measured according to Eq. (38).

$$\Omega_{TEG} = \frac{m(t) - m_{dry}}{m_{dry}} \tag{38}$$

where $m(t)$ is the mass at a given time [g] and m_{dry} is the dry sample mass [g].

The flasks containing the samples and the TEG were kept at room temperature during the period of investigation. For each membrane type, duplicates were measured in order to strengthen the statistical significance of the measurement.

To determine the transport properties of the thin composite membrane, pervaporation tests were performed using an in-house built apparatus. Details on the pervaporation setup are given elsewhere [48]. The membrane was placed inside the sample holder and the liquid solution was circulated on the top of the membrane. At the same time, vacuum was created on the downstream side by a vacuum pump, monitoring the pressure using a pressure transducer with a 100 mbar full scale. Initially, the system was running for at least 1 h to allow the achievement of steady state conditions across the membrane. Afterwards, the permeate vapour was sent to the sampling trap, where it was collected due to the cold temperature created by the liquid nitrogen. The permeate mass was determined by weighing the sample holder and then collected for further GC analysis. To improve the statistical significance of the data, triplicates were measured for each temperature and feed liquid compositions. The pervaporation setup has a maximum temperature limit of 60°C. TEG/H_2O solutions used in the feed were prepared on a mass base by mixing different amounts of the two components. Information about the temperature and the different feed solutions used in the experiments are reported in Table 2.

When glycol mixtures were used as liquid feed, the analytical determination of the permeate composition was performed using an Agilent 7890A gas chromatograph (GC) coupled with an Agilent 5975C inert mass spectrometer (MS) operating in the selected ion monitoring (SIM) mode. The GC-MS was equipped with an Agilent CP7596 capillary column and a split liner injector, and used Helium as inert gaseous phase. To increase the accuracy of the analysis, an internal standard (TEG-MEE) was used for each measurement. Before the injection of the permeate samples from pervaporation, standards were prepared with concentration ranging from 20 to 1000 ppm and used to create the calibration curve. More details about the GC analysis can be found elsewhere [49].

Upon the determination of the composition of the permeate samples, the molar flux of water [g/m^{s}s] can be determined according to Eq. (39)

$$J_{H_2O} = \frac{m_{tot}\omega_{H_2O}}{A_m t} \tag{39}$$

m_{tot} is the total permeated mass [g], ω_{H_2O} is the water mass fraction [$-$] as calculated from the GC analysis, A_m is the permeation area [m^2] and t is the time used to collect the permeate sample [h].

The permeance can then be calculated by Eq. (40) based on the assumption that the main mass transfer resistance is the dense membrane layer.

$$\frac{\mathscr{P}_{H_2O}}{\delta_{mem,d}} = \frac{J_{H_2O}}{M_{H_2O}(x_{H_2O}\gamma_{H_2O}P^{sat}_{H_2O,T_{l,mem}} - P_{down})} \tag{40}$$

where $\mathscr{P}_{H_2O}$ is the H_2O permeability [kmol m/s m^2 kPa] (1 kmol m/s m^2 kPa correspond to $2.985 \cdot 10^{15}$ Barrer), $\delta_{mem,d}$ is the dense membrane layer thickness [m], x_{H_2O} is the mole fraction of H_2O in the feed liquid, γ_{H_2O} is the activity coefficient of H_2O, $P^{sat}_{H_2O}$ is the saturation pressure of H_2O [kPa] at the liquid inlet temperature and P_{down} is the downstream pressure [kPa].

Finally, the process selectivity ($\alpha_{H_2O/TEG}$) can be determined as:

$$\alpha_{H_2O/TEG} = \frac{y_{H_2O}/y_{TEG}}{x_{H_2O}/x_{TEG}} \tag{41}$$

where y_{H_2O} and y_{TEG} are the mole fraction of H_2O and TEG in the permeated vapour and x_{H_2O} and x_{TEG} are the mole fraction of H_2O and TEG in the feed liquid.

Table 2
Experimental pervaporation results for liquid feeds of pure H$_2$O, 70 wt%TEG, 80 wt%TEG and 90 wt%TEG. The membrane used is a composite membrane with a porous support layer of polypropylene Celgard ˚2400 (~25 μm) and a dense layer of Teflon ˚AF2400 (~1.7 μm).The higher TEG values detected for the solution containing 80 wt% are mainly related to contamination of samples.

Operation condition					Experimental results			Model calculated	Relative
Temperature [℃]	Downstream	Flow rate	Mole fraction	Weight fraction	Total flux	TEG content	H$_2$Opermeability	H$_2$Opermeabiltiy	errors
	pressure [mBar]	[L/h]	H$_2$O in feed	H$_2$O in feed	[g/m^{2}h]	[ppm]	[Barrer]	[Barrer]	[%]
29.6	3.40	0.55	1	1	121.6		2430	2785	14.6
29.7	3.39	0.55	1	1	122.2		2424	2775	14.5
29.6	3.40	0.55	1	1	122.1		2430	2785	14.6
39.1	3.84	0.55	1	1	203.6		2325	2695	15.9
39.2	3.84	0.55	1	1	197.4		2241	2585	15.4
39.2	3.81	0.55	1	1	199.4		2264	2618	15.6
39.3	3.82	0.55	1	1	201.3		2279	2635	15.6
51.1	4.45	0.24	1	1	344.1		2082	2485	19.3
51.2	4.49	0.24	1	1	353.7		2124	2545	19.8
51.3	4.51	0.24	1	1	354.1		2122	2540	19.7
30.0	3.16	0.96	0.79	0.31	75.0	126	2093	2410	15.2
30.0	3.17	0.96	0.79	0.31	77.6	74	2163	2502	15.7
30.0	3.51	0.96	0.79	0.31	75.7	77	2135	2465	15.5
39.6	3.46	0.96	0.79	0.31	124.8	78	1872	2170	15.9
39.6	3.46	0.96	0.79	0.31	122.3	117	1834	2120	15.9
39.5	3.93	0.96	0.79	0.31	124.2	77	1892	2195	16.0
50.4	3.21	0.96	0.79	0.31	197.1	152	1597	1860	16.5
50.4	3.87	0.96	0.79	0.31	206.2	225	1679	1970	17.3
29.7	2.98	0.62	0.69	0.21	48.8	932	1740	2010	15.5
29.7	2.97	0.62	0.69	0.21	48.5	1087	1726	1995	15.6
29.7	2.98	0.62	0.69	0.21	52.0	641	1859	2165	16.4
39.4	3.20	0.62	0.69	0.21	84.9	811	1589	1873	17.8
39.4	3.17	0.62	0.69	0.21	83.2	543	1555	1825	17.4
39.4	3.19	0.62	0.69	0.21	77.4	778	1451	1685	16.1
51.0	3.52	0.62	0.69	0.21	141.0	828	1333	1592	19.5
51.0	3.50	0.62	0.69	0.21	136.0	539	1286	1530	18.9
50.9	3.49	0.62	0.69	0.21	133.9	811	1269	1505	18.6
29.7	2.90	0.93	0.49	0.10	31.9	113	1939	2360	21.7
29.7	2.89	0.93	0.49	0.10	31.0	73	1882	2280	21.1
29.7	2.88	0.93	0.49	0.10	31.0	71	1877	2275	21.2
40.0	3.03	0.93	0.49	0.10	54.1	90	1613	1990	23.4
39.9	3.03	0.93	0.49	0.10	52.5	100	1570	1925	22.6
49.8	3.21	0.93	0.49	0.10	80.2	414	1316	1640	24.6
49.7	3.18	0.93	0.49	0.10	80.3	598	1322	1650	24.8
49.7	3.58	0.93	0.49	0.10	80.5	581	1333	1665	24.9

3.2. Experimental results

3.2.1. Compatibility test

In subsea operations, reliability and long-term stabilities are key priorities. Therefore, compatibility tests are fundamental to identify suitable candidates for the thin dense layer to be coated on the top of the porous support. Compatibility has been estimated by means of immersion tests, identifying the amount of TEG absorbed within the polymer matrix. High TEG uptake would lead to significant swelling phenomena, affecting the long-term performance of the membrane. In addition, large TEG concentration in the membrane could possibly lead to poor TEG recovery after the pervaporation stage.

To achieve high efficiency of water removal, the dense layer must own a high water permeability. According to this idea, two family of materials were investigated: hydrophilic membranes with hydrophobic backbones (Nafion and Nexar); hydrophobic membranes with high free volume (Teflon ˚AF2400, PIM-1, 6FDA-Durene, PTMSP, PDMS). In the first case, the hydrophilic side chains are able to ensure high water permeability and the hydrophobic backbones confer good mechanical stability under swollen conditions [50,51]. In the second group, the membrane integrity is guaranteed by the hydrophobic nature, but the high free volume ensure large transmembrane fluxes [48,52]. Fig. S2 (Supplementary material) displays the data observed for the different polymeric samples prepared. Both hydrophilic membranes showed high TEG uptake: Nexar showed an equilibrium value of about 1.75 g$_{TEG}$/g$_{pol}$, whereas about 1 g$_{TEG}$/g$_{pol}$ was measured in the case of Nafion. In

both cases, the sulfonic groups are considered responsible for interactions with the hydroxyl groups present in the glycol. The larger uptake of Nexar is likely related to the higher sulfonic content compared to Nafion. Among the hydrophobic high free volume polymers, PIM-1 showed the highest TEG uptake, with a value close to one observed for Nafion, followed by PTMSP and 6FDA-Durene, in which the uptake was measured to be in the range of 0.75 g$_{TEG}$/g$_{pol}$. On the contrary, low TEG uptake was observed in the case of PDMS and Teflon ˚AF2400. In particular, PDMS showed an uptake in the order of 0.05 g$_{TEG}$/g$_{pol}$, whereas negligible uptake was observed in the case of Teflon ˚AF2400. In this last case, the results may be attributed to the high hydrophobic nature of the carbon-fluoro bonds present on the polymer structure. A negligible TEG uptake is a promising precondition to achieve long-term stability of the pervaporation unit in a wide range of operating conditions, satisfying a key premise in subsea operations. In addition, despite the hydrophobic nature, the high free volume is supposed to ensure high H$_2$O permeance possibly limiting the interfacial area needed to achieve the target separation. In this regard and according to the results obtained from the compatibility test, Teflon ˚AF2400 appeared to be the most suitable material to match the project requirements and, therefore, it was chosen for further investigation.

3.2.2. Pervaporation test

The results obtained from pervaporation tests are reported in Fig. 2a and in Table 2. By increasing the operating temperature, the transmembrane flux increased for all the investigated feed solutions. In the
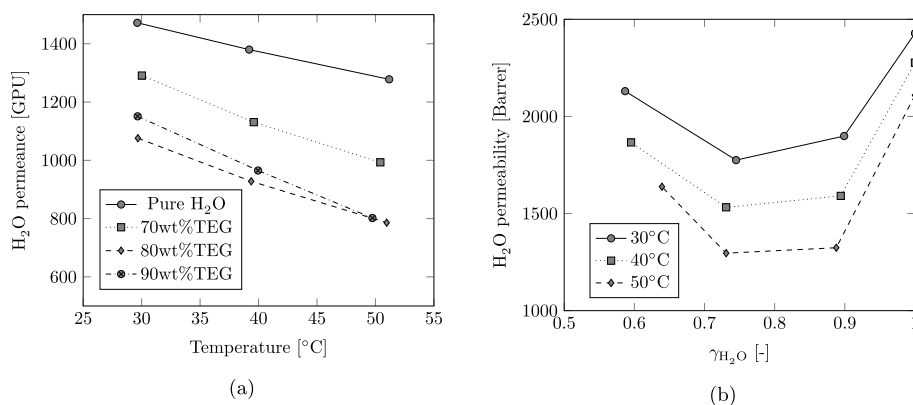
Fig. 2. (a) The calculated H_2O permeance for the dense Teflon ®AF2400 layer ($\sim 1.7\,\mu m$) form the result at different operation temperatures and feed compositions. (b) The calculated H_2O permeability as a function of H_2O activity coefficient (γ_{H_2O}) at different temperatures.

case of pure H_2O, the total flux increased from $120\,g/m^2$ h at 30°C to $350\,g/m^2$ h at 50°C. The positive variation is mainly related to the larger equilibrium pressure (i.e., driving force) of H_2O at higher temperature. For binary H_2O/TEG mixtures, the flux decreased proportionally to the water concentration in the feed mixture. At 30°C, the value ranged from $\sim 75\,g/m^2$ h at 70 wt% TEG to $\sim 31\,g/m^2$ h at 90 wt% TEG. However, the determination of the permeate composition showed an extremely low TEG concentration, within the ppm range (Table 2). Despite the challenges of measuring such low concentration through GC-MS, the values ranged from 70 to about 500 ppm, showing increasing trend with operating temperature and TEG concentration in the feed solution. In the case of the solution containing 80 wt% TEG, the higher TEG values detected are mainly related to contamination of the samples. Upon the determination of the TEG concentration in the permeate, the H_2O permeance has been calculated according to Eq. (40) and the results are reported in Fig. 2a. In this case, the increase of temperature determined a drop in the H_2O permeance value, suggesting that the flux increment is smaller than the driving force enhancement. Despite the glassy nature, the high free volume of Teflon ®AF2400 determines that its permeability is dominated by the solubility coefficient. Similar trend have been observed also for CO_2 and primary amines [48]. For pure H_2O, a permeance between 1500 and 1300 GPU was observed. The use of H_2O/TEG binary mixture as feed solution, determined an additional decrease of the permeance value, possibly related to competitive sorption within the polymeric matrix. Similarly to the case of total flux, the drop appeared proportional to the water content in the feed solution. Despite the contamination observed for 80 wt% TEG solution, the low concentration of TEG in the permeate sample allowed the calculation of H_2O permeance for this data series, with negligible effect on the accuracy of the reported value. At 30°C, the permeance decreased to 1290, 1151 and 1075 GPU for TEG concentraton of 70, 80 and 90 wt% TEG, respectively. For the three investigated operative temperatures, the H_2O permeance trends clearly showed a flattening for low water content in the feed solution.

Fig. 2b shows the different H_2O permeability values as a function of the H_2O activity coefficient (γ_{H_2O}) for the given liquid phase use in the pervaporation experiments. In the case of pure H_2O, at 30°C, a value of 2428 Barrer is obtained and further increase of temperature determined a decrease of the H_2O permeability to 2277 and to 2109 Barrer at 40 and 50°C, respectively. This result agrees well with the data previously published from our group for self-standing Teflon ®AF2400 membranes [48]. Minor differences may arise by the different thickness of the Teflon ®AF2400 layer, which have been demonstrated to affect the gas permeability for condensable gases such as CO_2 [53]. The results are also in the same order of magnitude of the value indicated in technical datasheet [54] from the producer (Chemours) for H_2O permeability (4000 Barrer). However, due to the limited amount of information provided in the datasheet, it is difficult to explain the differences

between our results and the one reported by the supplier. Scholes et al. [55] also observed significant differences between the H_2O permeability value they measured in Teflon ®AF1600 and the one reported in the datasheet. They rightfully suggested that the reason is the film casting and annealing history of the sample. When TEG/H_2O mixture were used as liquid feed, the H_2O permeability showed a 10–40% decrease compared to the pure H_2O value, showing however an increase for the lowest water activity investigated. For a given composition of the liquid feed, the results followed an Arrhenius trend (linear regression coefficient > 99%) and it has been possible to calculate the activation energy of H_2O permeation. For pure water a value of $-5.3\,kJ/$ mol is obtained. Scholes et al. measured a larger value (65 kJ/mol) for Teflon ®AF1600 [55], but differences are well-explained by the much larger free volume of Teflon ®AF2400, which reduce the thermal activation of the diffusion coefficient. At increasing TEG content, the permeation appeared to be more thermally activated, in view of the increase of the activation energy to 10.5, 10.2 and 14.6 kJ/mol at 30, 20 and 10 wt% of H_2O in TEG, respectively.

In addition to the H_2O permeance, the determination of the permeate concentration allowed also to calculate the separation factor according to Eq. (41). Fig. S3 (Supplementary material) shows the results achieved for the H_2O/TEG binary mixtures, with a comparison to the separation determined by the vapour-liquid equilibrium. Even though negligible effects on the separation factor can be associated to the presence of the membrane in the high water concentration range (30 wt% H_2O in the feed), at the low water content (10 wt% H_2O in the feed) the overall value is significantly increased. According to this result, the use of a hydrophobic membrane can possibly lead to improved TEG recovery, and therefore to lower operational costs associated to the regeneration process of the absorbent as the operation conditions would be in the lower water content range. However, the benefits of the membrane appear to be reduced with increasing operating temperature. The membrane was tested over a period of 3 months and the H_2O permeance was reduced with less then 10% [49].

As previously mentioned, only one literature reference is available for TEG dehydration [18], using silica membranes. In the research, they reported a water flux value corresponding to $184\,g/m^2$ h, obtained at 80°C and using 9 wt% water in the feed. By extrapolating the H_2O flux value obtained for the 90 wt% TEG solution at 80°C (linear correlation), the Teflon ®AF2400 composite membrane is expected to achieve a value of $152\,g/m^2$ h, which is comparable with the results obtained using inorganic membranes. Within the family of hydrophobic high free volume polymers, PIM-1 has also been investigated for the dehydration of glycols (MEG [13]). Similar H_2O permeances are reported in the study (1000–2000 GPU for water content between 6.5 and 22 wt%), although a much thicker membrane (30 μm) was used. However, the analysis of the permeate concentration determined that PIM-1 is MEG selective, with MEG permeance that are about one order of magnitude higher

compared to the H_2O permeance. As highlighted by our compatibility study, this effect can be generated by the high glycol uptake that characterized PIM-1, corroborating our idea that choosing a dense layer with negligible glycol uptake can lead to better stability and absorbent recovery.

3.3. Model tuning

The unknown parameter in the model is the dense membrane permeability. It is therefore a need for a permeability correlation for the model. Experimental data from a pervaporation apparatus was used. It would be more difficult to test the material properties by thermopervaporation experiments as many steps are involved. It is expected that the permeability correlation developed from pervaporation can be used in the thermopervaporation model, as the permeability of the dense layer is a material property. When changing from a pervaporation system to a thermopervaporation system the difference is the boundary conditions, which are considered in the model, and the membrane properties are expected to be unchanged. However, to be able to tune the model with experimental data the developed model was adjusted to fit the experimental apparatus. The main changes are:

- The experimental apparatus only consist of one feed channel with membrane on one side and a wall on the other (Illustrated in Fig. S4, Supplementary material).
- Vacuum pump is used downstream, so no cooling water is used. The downstream pressure is specified based on experimental data.
- Temperature at the wall is assumed equal to the feed temperature as the experiment is performed inside a temperature-controlled environment.
- Adiabatic conditions are assumed ($Q = 0$). Therefore, only heat of vaporization is considered.

There are some deviations between the model and the experimental apparatus, which should be mentioned. In the apparatus, the geometry of the flat membrane is a circle and the feed is entering in one point. In the model, the membrane geometry is a square with the same membrane area as in the pervaporation experiments. In addition, uniform conditions along the inlet of the membrane ($z = 0$) is assumed which might give some deviation between the model and the experimental results.

The theoretical model developed for the pervaporation apparatus was validated against experimental data for the porous polypropylene (PP) membrane. In these experiments, pure water was used as the addition of TEG could provide wetting problems for the porous membrane. Two different mass transfer models were evaluated for the porous membrane. The first one is mass transfer by molecular diffusion, while the second includes the Knudsen diffusion in addition to the molecular diffusion. As can be seen from Fig. 3 the Knudsen diffusion has a significantly effect on the water transport over the membrane. With Knudsen diffusion included in the model, it is shown a good agreement between the model and the experimental data, within a mean error of -9%. The variation in the model results at the same temperature is due to the change of downstream pressure for the different experiments, which will affect the driving force in the model and hence the predicted flux.

When a composite membrane is used and the main mass transfer resistance is in the dense layer the Knudsen diffusion does not show a significant effect on the results. Increasing the permeability of the dense layer results in more contribution from the porous support to the total mass transfer resistance, and hence the Knudsen diffusion gets more important. Therefore, Knudsen diffusion should be included in the flux equation for this system. Based on the validation of the porous support, it is reasonable to assume that the unknown parameter for model tuning is the permeability of the dense layer.

The experimental results for the composite membrane consisting of a $25\,\mu m$ thick porous polypropylene substrate coated with a $1.7\,\mu m$ thick dense layer of Teflon °AF2400 and the operation conditions are given in Table 2. In the present model, only H_2O permeation is considered as the TEG flow is expected to be extremely small compared to the water, based on the high separation factor (Fig. S3, Supplementary material). Furthermore, the H_2O permeability is measured using mixtures, and the effect of TEG on the H_2O permeation is therefore considered. An alternative method for permeability calculation to avoid the assumption of the dense layer being the main resistance and to include the effect of the liquid phase and the porous support is to use the developed model for the pervaporation apparatus to find the permeability value. In this evaluation the experimental feed conditions and downstream pressure is used and the permeability value is adjusted and optimized to achieve an equal value between the experimental flux and the predicted flux from the model. An assumption for this calculation method is that the dense layer is the only unknown parameter in the model. The predicted permeability values based on the model is given in Table 2. The deviation between the permeability calculated from the experimental result and with the use of the model is about 14–25%. These results seem to be reasonable as it is expected that the liquid phase and porous support will have some contribution to the mass transfer resistance. It is therefore expected that the model predicted permeability should be somewhat higher than the experimental calculated permeability. In addition, with this calculation method all uncertainty in the model is included in the permeability value.

When going from pure H_2O liquid feed to introduce TEG, several factors are changing and will affect the system. Increasing TEG amount in the feed will change the viscosity of the liquid and the diffusivity of H_2O in TEG, affecting the mass transfer. When all these effects are taken into consideration, the permeability results indicate that the permeability is temperature and concentration dependent, as illustrated in Fig. 4.

As it can be seen from Fig. 4, the permeability value is showing a plateau for mole fractions of H_2O lower than 0.7 (80 wt% TEG solution). The effect of TEG on the H_2O permeability can possibly be the reason of the observed trend. It is clear that the TEG will influence the H_2O permeability as it is proven that we have some TEG flux, even if this is very low. By looking at the activity coefficient of TEG in TEG-H_2O solution (Fig. S5, Supplementary material), the activity coefficient of TEG is small at low TEG content, and hence the effect of TEG on H_2O permeability is expected to be low. The TEG activity coefficient curve has a rapid increase when TEG is added to the pure H_2O, but the increase is getting lower after 0.7 mol fraction H_2O that is the same conditions as when the permeability value is flattening out. A suggested explanation to these results are that when the TEG content is increasing the activity coefficient is increasing giving more effect on the permeability (as the TEG absorption in the membrane material is increase). When the H_2O mole fraction is above 0.7, a further increase in the TEG content gives a smaller change in the TEG activity coefficient. At these conditions, the amount of TEG is still affecting the permeability, but the activity coefficient and hence the amount of TEG absorbed in the membrane material is not significantly changed, which results in a more constant permeability value.

It would be favourable to include a permeability correlation in the model for prediction of the permeability value at the given operation condition of the model. The experimental results show that the permeability of the dense layer is both dependent on the temperature and the H_2O concentration. As it can be seen from Fig. 4, there is a concentration dependency between 0.7 and 1 mol fraction H_2O. Below this concentration, the permeability value is not largely affected by the concentration. Therefore, the correlation developed at $x_{H_2O} < 0.7$ follows the Arrhenius equation with only temperature dependency. The model calculated permeability values of the dense Teflon °AF2400 membrane in Barrer at 80 wt% TEG and 90 wt% TEG experiments have been used in the development of a temperature dependent correlation as given in Eq. (42). The parameters A_1 and A_2 in the correlation are
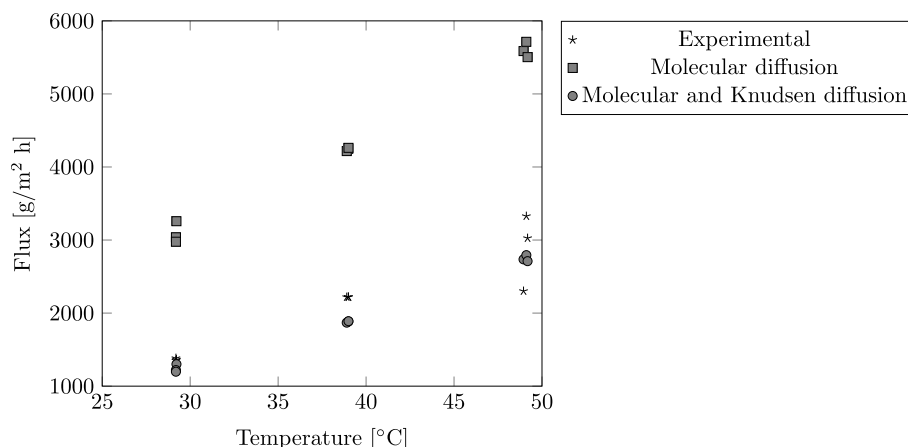
Fig. 3. Comparison between experimental flux data for a porous polypropylene membrane (25 μm) with the model predictions with two different diffusion cases; one with only molecular diffusion and the second with both molecular and Knudsen diffusion.
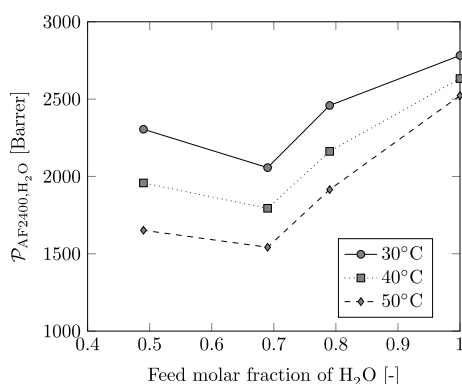

Fig. 4. Average model predicted permeability values as function of feed H_2O content at different temperatures.

Fig. 5. Permeability correlation model with 95% confidence interval vs model predicted permeabilities from experimental data.

Table 3
The values of the parameters in the permeability correlation found by optimization to experimental data, in addition to a 95% parameter confidence interval.

Parameter	Value	95% Conf. Interval	
		Low limit	Upper limit
A_1	16.445	-6.645	39.535
A_2	12302	8681.3	15923

found based on optimization of the model to experimental results. Table 3 gives the parameter values with a 95% confidence interval.

$$\mathscr{P}_{\text{AF2400,H}_2\text{O,Barrer}} = A_1 \exp\left(\frac{A_2}{R_g T}\right) \tag{42}$$

The developed correlation predicts the permeability values within an absolute average error of 4.4% compared to the model calculated permeabilities (Fig. 5). With the assumption that the model structure is correct, the model prediction for the permeability with a 95% confidence interval is given in Fig. 5, which includes the variation in the model. This plot is of interest as the model is developed based on experimental data at temperatures between $30 - 50°C$, while the operating conditions for the process will be at a higher temperature and extrapolation of the correlation will be used. It is therefore of interest to see the uncertainties of the model in the region of operation. Experiments are not performed at higher temperatures due to experimental limitations.
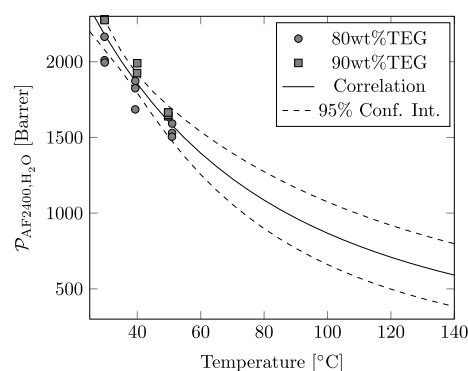
4. Sensitivity study

The permeability correlation developed in the study was implemented in the thermopervaporation model and the effect of different membrane module properties and operation condition on the separation performance was investigated. The sensitivity study is performed by evaluating one parameter at the time if nothing else is specified. By understanding the effect of the different module parameters and operation conditions on the separation performance, the critical design parameters, and operation conditions can be found. The developed model is valid for the plate-and-frame module configuration, but not for other configurations. The basis values for the membrane module properties and operation conditions used in the sensitivity study are given in Table 4.

4.1. Sensitivity of permeability correlation

A permeability correlation is used in the model, and a 95% confidence interval for the correlation gives some variation in the permeability value (Fig. 5). It would therefore be of interest to evaluate the effect of the permeability value on the separation performance. In this case study, the permeability value from the correlation is adjusted with a factor ($f_{\mathscr{P}_{\text{AF2400,H}_2\text{O}}}$) with different percentages and the effect on the separation performance is evaluated. As shown from the result (Fig. S6, Supplementary material), the effect on the separation performance is as expected, but not directly correlated with the adjustment factor. Increasing the permeability with 90% only increases the separation performance by 4.5%. The effect is lager when the permeability is reduced, which is expected as the resistance will be increased. However, with a 90% reduction of the permeability value the separation performance

Table 4
Membrane and operation parameters used for sensitivity study.

Parameter	Symbol	Value	Unit
Feed channel thickness	δ_f	4	mm
Air gap	δ_ag	10	mm
Cooling water channel thickness	δ_cw	5	mm
Number of feed channels	n_channels	2000	
Membrane length	L	1	m
Membrane width	L_w	1	m
Membrane thickness (dense)	$\delta_\text{mem,d}$	1	μm
Membrane thickness (porous)	$\delta_\text{mem,p}$	25	μm
Membrane porosity	ε_p	0.41	
Temperature liquid	$T_\text{l,feed}$	90	˚C
Temperature cooling water	$T_\text{cw,feed}$	4	˚C
Pressure liquid	$P_\text{l,feed}$	1	bar
Liquid flow	f_TEG	0.043	kmol/s
Mole fraction of H_2O in liquid feed	x_H2O	0.2261	
Cooling water average velocity	$v_\text{cw,av}$	0.1	m/s
Thermal conductivity AF2400 [56]	λ_AF2400	0.05	W/mK
Thermal conductivity PP [57]	λ_PP	0.15	W/mK

decreases by 21.3%. These results show that an error in the permeability correlation would not significantly change the separation performance.

4.2. Membrane thickness

In membrane separation, reducing the membrane thickness is normally favourable from a separation point of view. In the thermopervaporation process, the heat transfer between the hot liquid to the cooling water should be minimized. It is therefore of interest to evaluate if the membrane material with good thermal insulation would reduce the liquid temperature drop and how this would affect the separation performance. As shown from the results in Fig. S7 (Supplementary material), increasing the thickness of the membrane layers results in reduced temperature drop, but it also reduces the separation performance. The results indicate that the thickness of the porous support affects the separation performance, but less than the dense membrane layer thickness; the temperature drop is reduced more with the porous support thickness compared to the dense layer thickness. An increase of the porous support thickness from $25\,\mu$m to $1000\,\mu$m, keeping the dense membrane layer at $1\,\mu$m, results in a separation performance reduction of 10.5%, while the temperature drop is decreased with 13.7%. The effect of the dense membrane layer on the separation performance is more significant when changing from $1\,\mu$m up to $10\,\mu$m (porous support $25\,\mu$m), compared to further increase as the separation performance is almost negligible with higher thickness. With a dense layer thickness of $10\,\mu$m, about 6% of the H_2O in the liquid feed is removed under the given operation conditions and module design. This indicates that thin membranes are favourable in the thermopervaporation system, but there is a limitation related to processability and membrane stability.

4.3. Feed channel thickness

The effect of the feed channel thickness, which is the distance between the two membrane surfaces, on the separation performance was evaluated. In this investigation, the flow velocity changes along with the feed channel thickness (Fig. S8, Supplementary material), as the feed flow amount is kept constant. The results indicate that increasing the channel thickness will decrease the separation performance and the H_2O content in the outlet liquid is increased. Smaller channels provide shorter diffusive pathways from the center line of the channel to the membrane, resulting in less temperature (Fig. 6b) and concentration gradients (Fig. 6a) in the feed channel and hence increased separation performance. A reduction in the temperature results in a increased

permeability value which gives an reduction in the mass transfer resistance provided by the dense layer. In addition, the increased concentration gradient gives an increase in the mass transfer resistance provided by the liquid (0.2 mm Fig. 6c and 10 mm Fig. 6d). It is expected that the pressure drop of the liquid over the membrane module will increase with smaller feed channels, which is also shown from the results (Fig. S8, Supplementary material). From this evaluation, it seems that smaller channels are preferred, but the selection is restricted by liquid pressure drop and practical considerations such as solid impurities in the liquid, which might block the channels.

4.4. Air gap

Liquid temperature drop along the membrane module is a limiting factor, as it will reduce the driving force over the membrane. The temperature drop is a result of two different aspects: the heat transfer due to temperature differences from the hot TEG feed to the cooling water (Q_T) and the heat required for evaporation of the H_2O passing the membrane (Q_H). As illustrated in Fig. 7a, the heat transfer from hot to cold liquid dominates the temperature drop in the TEG phase. When the air gap, which is the distance from the membrane surface to the cooling wall, is increased the heat transfer is reduced as it is inversely proportional to the air gap spacing, but it is still dominant. This shows the importance of the air gap and the heat insulation to reduce the heat transfer from hot liquid to the cold cooling water. An evaluation of the effect of the air gap was done by only changing this parameter in the system. As can be seen from Fig. 7b and c, the separation performance is improved as expected when the temperature drop along the module is reduced. The effect on the separation performance is more significant when the air gap is changed from 5 mm to 10 mm, compared to further increase after 10 mm. Increasing the air gap will result in larger membrane modules despite of better separation performance. Therefore, a trade-off between increased separation performance and module size can be identified. This investigation has shown that the air gap is a critical parameter in the design and development of the thermopervaporation membrane module.

4.5. Membrane length

Increasing the membrane length results in enlarged membrane area for mass and heat transfer. As shown earlier, the dominant reason for temperature reduction in the liquid feed is the heat transfer from the hot liquid to the cold cooling water. The temperature drop for the liquid along the module is increasing with the heat transfer area, as shown in Fig. 8. As the temperature of the liquid is decreasing, the equilibrium partial pressure of H_2O decreases and as can be seen the H_2O flux is reversed with a membrane length above 2 m. From this evaluation it can be assumed that under the given membrane parameters and operation conditions the optimum membrane length is 2 m, which correspond to a membrane area of 8000 m^2 (membrane width 1 m and 2000 feed channels).

4.6. Cooling water channel thickness

The effects of the cooling water channel thickness at different cooling water velocities were investigated to understand the effects on the pressure drop and cooling water temperature, which are of interest with respect to energy consumption. Fig. S9 (Supplementary material) indicates that a higher velocity is favourable to reduce the temperature increase, while for the pressure drop lower velocity is preferred. For a velocity of 0.01 m/s and a cooling water channel thickness of 0.5 mm, the temperature increase is about 19˚C, which is shown to have an effect on the separation performance. From this investigation, it seems that a velocity of 0.05 m/s or higher will prevent the temperature increase. In addition, a cooling water channel thickness of 2 mm or more seems not to affect either the separation performance, the temperature
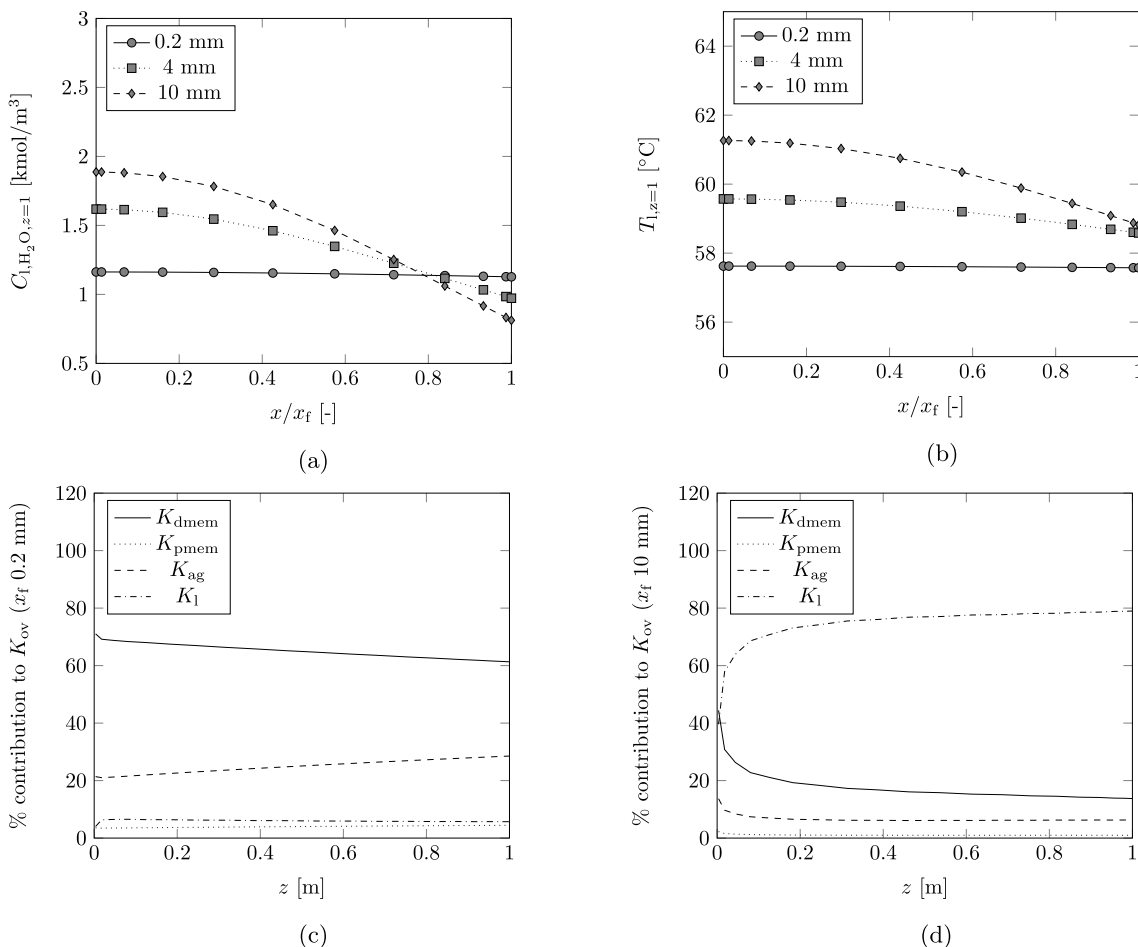
Fig. 6. (a) Concentration gradients and (b) temperature gradient in x-direction at different feed channel thickness, where $x/x_f = 0$ represent the center of the feed channel and $x/x_f = 0$ represent the liquid membrane. The contribution of the liquid phase (K_l), the dense membrane layer (K_{dmem}), the porous support (K_{pmem}) and the air gap (K_{ag}) on the total mass transfer resistance (K_{ov}) with a feed channel thickness of (c) 0.2 mm and (d) 10 mm.
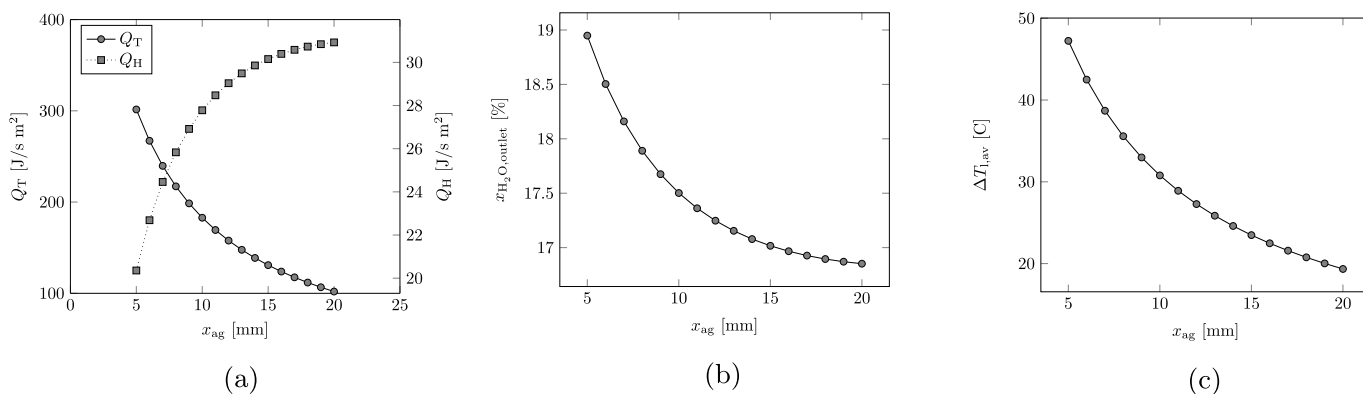

Fig. 7. (a) Heat transfer from the hot liquid to the cooling water (Q_T) and the heat spent for evaporation of the H_2O passing through the membrane (Q_H) as a function of the air gap (distance between membrane surface and cooling wall). (b) Effect of changing the air gap width on the separation performance and (c) on the temperature drop along the membrane module.

or the pressure drop.

4.7. Cooling water temperature

The previous evaluation shows that the increase in cooling water temperature along the membrane module does not largely affect the separation performance. Therefore the effect of the inlet cooling water temperature was investigated. When the cooling water temperature is increased, a reduction in the temperature drop could be seen, as shown

in Fig. 9a. This is expected, as the driving force (temperature difference) over the membrane will be reduced. A smaller temperature drop of the liquid feed provides a higher equilibrium H_2O pressure in the liquid solution, however as the downstream saturation pressure is increased with increasing cooling water temperature the separation performance is reduced with higher cooling water temperature (as shown in Fig. 9b). Less effect of the cooling water temperature is shown when the TEG feed temperature is increased. For subsea operations, the availability of seawater at about 4°C for cooling purposes is a large advantage, and
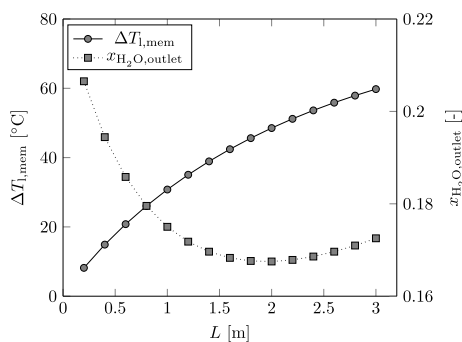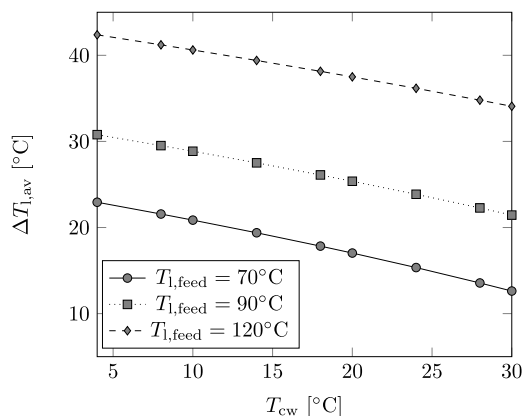
Fig. 8. The effect of the membrane length on the temperature drop in the liquid over the membrane module and the amount of H_2O in the outlet of the liquid.

Fig. 10. The effect of the TEG molar flow on the H_2O content in the liquid outlet of the membrane module and the temperature drop over the membrane module length.

increasing the cooling water temperature will be inefficient.

As it was shown that the effect of increasing the temperature from 4 to 10°C did not significantly change the separation performance, at least not at higher feed temperatures, an alternative module design was evaluated. The changes in the module design are that the cooling water channels are replaced with cooling plates only and the cooling water circulation loop is located outside the module. To be able to remove all the heat from the cooling plate sufficient heat transfer area is assumed to be installed at the end of the cooling plate outside the module with an external cooling water circulation loop. In this evaluation the temperature on the inlet and outlet of the cooling wall (z = 0 and z = L) is set to 5°C. Fig. S10 (Supplementary material) shows that removing of the cooling water channel inside the module would give a reduction in the separation performance. The reason for this is the increased temperature of the cooling plate inside the module at the interface to the air gap. Different thermal conductivities were tested and the results showed that with materials such as stainless steel, the thermal conductivity is too low and the temperature increase along the cooling wall is too high, which leads to reversed mass transfer. For this module design a material with high thermal conductivity around 400–500 W/m^2 K is required, and possible materials could be silver [58] or graphite [59]. However, as shown the separation performance is lower than when a cooling water channel is introduced even with the high thermal conductivity. In addition, for this evaluation 5°C was used as the cooling wall inlet and outlet temperatures, but it might be more realistic to think that this temperature will be slightly higher and then the performance would be even more reduced compared to the reported values.

The idea behind this design was that the pressure drop in a outside cooling water loop could possibly be lower that the inside cooling water
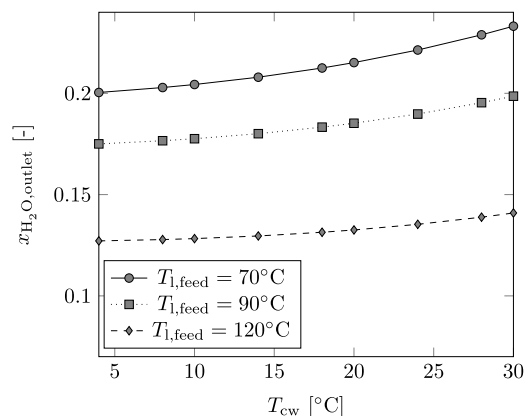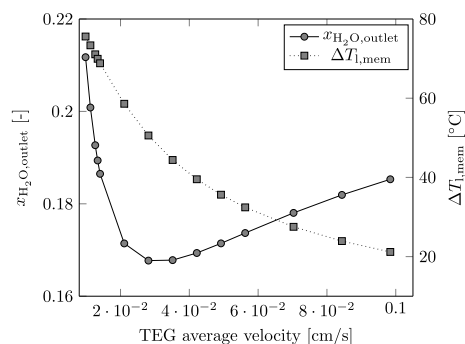
channels. It would then be an evaluation if a higher investment cost, which is a one-time investment, would be favourable compared to operation cost due to energy requirements during operation. However, as can be seen from the previous investigation of the cooling water channel thickness, in Fig. S9, the pressure drop along the channel is very small. Based on this and the fact that the separation performance is higher with a cooling water channel, the original module design would be favourable for the system.

4.8. TEG feed temperature

As this system is evaluated for subsea operation, it is favourable to keep the heating requirements as low as possible. It could also be an advantage if the required heat for the feed liquid can be provided with heat integration from the system. It is therefore of interest to see how the separation performance is changed with the feed liquid temperature. Higher feed temperature gives a larger temperature difference between the feed and the cooling water, which as expected results in increased temperature drop over the membrane module, as indicated in Fig. S10 (Supplementary material). However, the H_2O content in the TEG outlet is reduced with increasing temperature. The reason for this is that the equilibrium partial pressure is increased with a higher temperature, which enlarges the driving force for mass transfer over the membrane. Based on this evaluation high temperature is favourable from a separation point of view, but an evaluation should be done on energy demands to find the optimum temperature value. It is also important to consider the stability of the membrane material when selecting the optimum operation temperature. Furthermore, when thermopervaporation is considered for regeneration of TEG in a natural gas

Fig. 9. (a) Effect of cooling water inlet temperature on the temperature drop of the TEG phase along the membrane module and (b) the effect on the outlet molar fraction of H_2O.

dehydration process, the regeneration temperature and hence the purity of the regenerated TEG determines the water dew point for the dry natural gas. The regenerated TEG at 120°C has a water content of 12.7 mol%, which is not sufficient to achieve a dry natural gas with water dew point of −18°C at 69 barg. Therefore, in a dehydration process, multiple thermopervaporation units in series would be required with heating between the units to achieve the required purity of the TEG. The evaluation of regeneration temperature and the number of regeneration steps needed to reach a suitable amount of H_2O in the natural gas is an optimization problem, which is reported elsewhere [60].

4.9. Liquid velocity

For a given set of membrane properties and operation conditions an increase in liquid flow rate results in reduced residence time for the liquid in the membrane module as the liquid velocity is increased. As illustrated in Fig. 10, according to the given module configurations and operation conditions, an optimum liquid velocity around 0.03 cm/s is found. The reason for this optimum velocity is that at these conditions equilibrium is achieved at the outlet of the membrane module. At higher velocities the equilibrium is not achieved, the residence time is lower and the separation performance is reduced. With lower velocities than 0.03 cm/s the residence time in the module is too high, giving a large temperature drop, which results in the driving force being reverse. At lower velocities, a shorter membrane module and hence less membrane area is required to achieve the same separation performance. These results show that the liquid velocity should be optimized together with the module design, where it is important to considered the maximum allowable temperature drop for the liquid.

5. Conclusion

In the present study, the potential of membrane thermopervaporation for regeneration of TEG has been evaluated from both the experimental and modelling point of view. A compatibility study showed that among several polymeric materials, only PDMS and Teflon °AF2400 have been found to absorb limited amount of TEG, meeting the requirement for stability on long-term operation required for subsea applications. The latter polymer has been chosen for further characterization and, despite the hydrophobic nature it shows water fluxes that are comparable with the value obtained from inorganic membranes. Furthermore and most importantly, the H_2O/TEG separation factor appeared to be improved with respect to the vapour-liquid equilibria in the low water content range, which is more representative of real conditions for TEG dehydration. These results imply a promising potential of improving TEG recovery by means of membrane pervaporation, and it can positively affect the operational costs associated to the natural gas dehydration.

Aiming at a throughout evaluation of the potential of the proposed technological solution, a mathematical model of the thermopervaporation module was developed. Initially, the model has been adjusted to a pervaporation system with downstream vacuum for tuning of the H_2O permeability value according to the experimental value. The correlation proposed for H_2O permeation through the proposed thin composite membrane showed an absolute average error of 4.4% and was further used for the development of the thermopervaporation model. The effect of varying membrane properties and operation conditions are clearly shown on the separation performance. In particular, the air gap is shown to be a critical parameter in the design of a thermopervaporation module. Liquid temperature drop is a limiting factor for the separation performance as the driving force will be reduced. The temperature drop is caused by the heat flux due to evaporation and the heat transfer between the hot and the cold liquid, where the latter being dominant. The air gap is important as an insulation layer for heat transfer, as the heat exchange is inversely

proportional with the air gap spacing. When the air gap is increased from 5 mm to 10 mm, the separation performance is increased with 6.7%. Further increase of the air gap will improve the separation performance, but to a smaller extend. In addition, the module size is proportional to the air gap that gives a trade-off between increased separation performance and module size.

The present research revealed a promising potential of using thermopervaporation technology to regenerate TEG. As part of future investigations, the experimental characterization of the thermopervaporation performance as well as the integration of the proposed thermopervaporation model in process simulation will be considered.

Acknowledgement

Appendix A. Supplementary data

Supplementary data to this article can be found online at https://doi.org/10.1016/j.memsci.2019.117205.

Nomenclature

A_m	Membrane area [m^2]
$A_1 - A_2$	Permeability model parameters
A, B, C, τ_γ	Activity coefficient model parameters
$C_{l,i}$	Molar concentration of component i in the liquid phase [kmol/m^3]
$C_{l,i,\text{feed}}$	Molar concentration of component i in the liquid feed [kmol/m^3]
$C_{p,cw}$	Heat capacity of the cooling water [J/kg K]
$C_{p,l}$	Heat capacity of the liquid phase [J/kg K]
D_{air,H_2O}	Diffusivity of H2O in air [m^2/s]
D_{kn,H_2O}	Knudsen diffusion [m^2/s]
$D_{l,i}$	Diffusivity of component i in TEG [m^2/s]
d_h	Hydraulic diameter of the feed channel [m]
d_p	Membrane pores diameter [m]
$f_{D,l}$	Friction factor
$f_{\mathscr{P}\text{AF2400},H_2O}$	Adjustment factor for the permeability correlation
L	Membrane length [m]
L_w	Membrane width [m]
J_i	Membrane flux of component i [kmol/m$_m^2$ s]
$J_{i,ag}$	Flux of component i over air gap [kmol/m$_m^2$ s]
$J_{i,dmem}$	Flux of component i over dense membrane [kmol/m$_m^2$ s]
$J_{i,pmem}$	Flux of component i over porous membrane [kmol/m$_m^2$ s]
K_{ag}	Air gas mass transfer resistance
$k_{ag,i}$	Air gap mass transfer resistance coefficient [m/s]
K_{dmem}	Dense memrbane mass transfer resistance
$k_{dmem,i}$	Dense membrane mass transfer resistance coefficient [m/s]
K_l	Liquid phase mass transfer resistance
K_{ov}	Overall mass transfer resistance
K_{pmem}	Porous membrane mass transfer resistance
$k_{pmem,i}$	Porous membrane mass transfer resistance coefficient [m/s]
M_{air}	Molecular weight of air [kg/kmol]
M_{H_2O}	Molecular weight of H2O [kg/kmol]
m_{dry}	Weight of dry membrane sample [g]
m_{tot}	Total permeate mass [g]
$m(t)$	Weight of membrane at a given time [g]
$n_{channels}$	Number of feed channels
P_{down}	Downstream pressure [kPa]
$P_{dmem,i}$	Equilibrium partial pressure of component i at porous-dense membrane interface [kPa]

P_l	Liquid phase pressure [kPa]
$P_{l,feed}$	Liquid feed pressure [kPa]
$P_{pmem,i}$	Equilibrium partial pressure of component i at porous membrane-air gap interface [kPa]
$P_{H_2O,T_{cw}}^{sat}$	H_2O saturation pressure at cooling water temperature [kPa]
$P_{H_2O,T_{l,mem}}^{sat}$	H_2O saturation pressure at liquid temperature at membrane interface [kPa]
$P_{l,i}^{VLE}$	Equilibrium partial pressure of component i at liquid-membrane interface [kPa]
$P_{ag,i}^{VLE}$	Equilibrium partial pressure of component i at air gap-condensate interface [kPa]
$\mathscr{P}_{AF2400,H_2O,Barrer}$	H_2O permeability [Barrer]
$\mathscr{P}_{H_2O}$	H_2O permeability [kmol m/s m^2 kPa]
Q	Total heat transfer from liquid to cooling water [W/m$_m^2$]
Re_l	Feed channel Reynolds number
R_g	Ideal gas constant [J/mol K]
$T_{ag,av}$	Average temperature in the air gap [K]
T_{cw}	Cooling water temperature [K]
$T_{cw,feed}$	Cooling water feed temperature [K]
T_l	Liquid temperature [K]
$T_{l,feed}$	Liquid feed temperature [K]
$T_{l,mem}$	Liquid temperature at membrane interface [K]
t	Time used to collect permeate sample [h]
v_{cw}	Cooling water velocity [m/s]
v_z	Liquid velocity [m/s]
$v_{z,av}$	Average liquid velocity [m/s]
x	Position in x-direction
x_{H_2O}	Molar fraction of H_2O in liquid
x_{TEG}	Molar fraction of TEG in liquid
y	Position in y-direction
y_{H_2O}	Mole fraction of H_2O in the permeate
y_{TEG}	Mole fraction of TEG in the permeate
z	Position in z-direction
$\alpha_{H_2O/TEG}$	Process selectivity
γ_{H_2O}	H_2O activity coefficient
$\Delta H_{vap,i}$	Heat of evaporation of component i [J/kmol]
δ_{ag}	Air gap spacing [m]
δ_{cw}	Cooling water channel thickness [m]
δ_f	Feed channel thickness [m]
$\delta_{mem,p}$	Porous membrane thickness [m]
$\delta_{mem,d}$	Dense membrane thickness [m]
ε_p	Membrane porosity
λ_l	Thermal conductivity of the liquid phase [W/m K]
λ_{cw}	Thermal conductivity of the cooling water [W/m K]
λ_{AF2400}	Thermal conductivity of AF2400 [W/m K]
λ_{PP}	Thermal conductivity of polypropylene [W/m K]
$\lambda_{mem,ag}$	Thermal conductivity of air in the membrane pores [W/m K]
λ_{ag}	Thermal conductivity of air gap [W/m K]
ρ_l	Liquid phase density [kg/m^3]
ρ_{cw}	Cooling water density [kg/m^3]
τ_p	Membrane tortuosity
Ω_{TEG}	TEG uptake in membrane material [g$_{TEG}$/g$_{pol}$]
ω_{H_2O}	Water mass fraction
Σ_v	Sum of atomic diffusion volumes

References

[1] R.M. Ramberg, S.R.h. Davies, H. Rognoe, O. Oekland, Steps to the subsea factory, OTC Brasil. October; Offshore Technology Conference, 2013 978-1-61399-287-6, pp. 29–31, , https://doi.org/10.4043/24307-MS http://www.onepetro.org/doi/10.4043/24307-MS.

[2] S. Mokhatab, W.A. Poe, J.G. Speight, Natural gas fundamental, Handbook of Natural Gas Transmission and Processing, 2006 978-0-7506-7776-9, pp. 1–28 chap. 1 http://www.sciencedirect.com/science/article/pii/B9780750677769500063 https://doi.org/10.1016/B978-075067776-9/50006-3.

[3] S. Mokhatab, W.A. Poe, J.G. Speight, Natural gas dehydration, in: S. Mokhatab, W.A. Poe, J.G. Speight (Eds.), Handbook of Natural Gas Transmission and Processing, Elsevier, 2006, pp. 323–364, , https://doi.org/10.1016/B978-075067776-9/50014-2 chap. 9 http://linkinghub.elsevier.com/retrieve/pii/B9780750677769500142.

[4] J.J. Carroll, Dehydration of natural gas, in: J.J. Carroll (Ed.), Natural Gas Hydrates, Elsevier, Burlington, 2009, pp. 151–169, , https://doi.org/10.1016/B978-0-7506-8490-3.00006-9 chap. 6 http://linkinghub.elsevier.com/retrieve/pii/B9780750684903000069.

[5] H. Lin, S.M. Thompson, A. Serbanescu-Martin, J.G. Wijmans, K.D. Amo, K.a. Lokhandwala, et al., Dehydration of natural gas using membranes. Part I: composite membranes, J. Membr. Sci. 413–414 (2012) 70–81, https://doi.org/10.1016/j.memsci.2012.04.009 http://linkinghub.elsevier.com/retrieve/pii/S0376738812003092.

[6] K. Dalane, Z. Dai, G. Mogseth, M. Hillestad, L. Deng, Potential applications of membrane separation for subsea natural gas processing: a review, J. Nat. Gas Sci. Eng. 39 (2017) 101–117, https://doi.org/10.1016/j.jngse.2017.01.023 https://doi.org/10.1016/j.jngse.2017.01.023.

[7] K. Dalane, H.F. Svendsen, M. Hillestad, L. Deng, Membrane contactor for subsea natural gas dehydration: model development and sensitivity study, J. Membr. Sci. 556 (March) (2018) 263–276, https://doi.org/10.1016/j.memsci.2018.03.033 https://doi.org/10.1016/j.memsci.2018.03.033.

[8] P. Shao, R. Huang, Polymeric membrane pervaporation, J. Membr. Sci. 287 (2) (2007) 162–179, https://doi.org/10.1016/j.memsci.2006.10.043 http://linkinghub.elsevier.com/retrieve/pii/S0376738806007095.

[9] R.W. Baker, Membrane Technology and Applications, second ed., John Wiley & Sons, Ltd, 0-470-85445-6, 2004.

[10] A. Basile, A. Figoli, M. Khayet, Pervaporation, Vapour Permeation and Membrane Distillation: Principles and Application, Elsevier Ltd, 978-1-78242-246-4, 2015 http://www.sciencedirect.com/science/book/9781782422464.

[11] A. Jonquières, R. Clément, P. Lochon, J. Néel, M. Dresch, B. Chrétien, Industrial state-of-the-art of pervaporation and vapour permeation in the western countries, J. Membr. Sci. 206 (1–2) (2002) 87–117, https://doi.org/10.1016/S0376-7388(01)00768-2.

[12] I.J.G. Wijmans, M. Park, J.G. Wijmans, A. Ng, A.P. Mairal, Natural Gas Dehydration Process and Apparatus, (2004).

[13] X.M. Wu, H. Guo, F. Soyekwo, Q.G. Zhang, C.X. Lin, Q.L. Liu, et al., Pervaporation purification of ethylene glycol using the highly permeable PIM-1 membrane, J. Chem. Eng. Data 61 (1) (2016) 579–586, https://doi.org/10.1021/acs.jced.5b00731 http://pubs.acs.org/doi/abs/10.1021/acs.jced.5b00731.

[14] Y. Wang, T.S. Chung, B.W. Neo, M. Gruender, Processing and engineering of pervaporation dehydration of ethylene glycol via dual-layer polybenzimidazole (PBI)/polyetherimide (PEI) membranes, J. Membr. Sci. 378 (1–2) (2011) 339–350, https://doi.org/10.1016/j.memsci.2011.05.020 https://doi.org/10.1016/j.memsci.2011.05.020.

[15] Y.T. Ong, S.H. Tan, Synthesis of the novel symmetric buckypaper supported ionic liquid membrane for the dehydration of ethylene glycol by pervaporation, Separ. Purif. Technol. 143 (2015) 135–145, https://doi.org/10.1016/j.seppur.2015.01.021 https://doi.org/10.1016/j.seppur.2015.01.021.

[16] M. Jafari, A. Bayat, T. Mohammadi, M. Kazemimoghadam, Dehydration of ethylene glycol by pervaporation using gamma alumina/NaA zeolite composite membrane, Chem. Eng. Res. Des. 91 (12) (2013) 2412–2419, https://doi.org/10.1016/j.cherd.2013.04.016 https://doi.org/10.1016/j.cherd.2013.04.016.

[17] R.R. Akberov, A.R. Fazlyev, A.V. Klinov, A.V. Malygin, M.I. Farakhov, V.A. Maryakhina, et al., Dehydration of diethylene glycol by pervaporation using HybSi ceramic membranes, Theor. Found. Chem. Eng. 48 (5) (2014) 650–655, https://doi.org/10.1134/S0040579514030014 http://link.springer.com/10.1134/S0040579514030014.

[18] H. van Veen, Y. van Delft, C. Engelen, P. Pex, Dewatering of organics by pervaporation with silica membranes, Separ. Purif. Technol. 22–23 (1–2) (2001) 361–366, https://doi.org/10.1016/S1383-5866(00)00119-2 http://linkinghub.elsevier.com/retrieve/pii/S1383586600001192.

[19] M. Hyder, P. Chen, Pervaporation dehydration of ethylene glycol with chitosan–poly(vinyl alcohol) blend membranes: effect of CS–PVA blending ratios, J. Membr. Sci. 340 (1–2) (2009) 171–180, https://doi.org/10.1016/j.memsci.2009.05.021 http://linkinghub.elsevier.com/retrieve/pii/S0376738809003780.

[20] M. Hyder, R. Huang, P. Chen, Composite poly(vinyl alcohol)–poly(sulfone) membranes crosslinked by trimesoyl chloride: characterization and dehydration of ethylene glycol–water mixtures, J. Membr. Sci. 326 (2) (2009) 363–371, https://doi.org/10.1016/j.memsci.2008.10.017 http://linkinghub.elsevier.com/retrieve/pii/S0376738808008971.

[21] D. Sun, P. Yang, H.L. Sun, B.B. Li, Preparation and characterization of cross-linked poly (vinyl alcohol)/hyperbranched polyester membrane for the pervaporation dehydration of ethylene glycol solution, Eur. Polym. J. 62 (2015) 155–166, https://doi.org/10.1016/j.eurpolymj.2014.11.027 https://doi.org/10.1016/j.eurpolymj.2014.11.027.

[22] G. Golubev, I. Borisov, E. Litvinova, V. Khotimsky, D. Bakhtin, A. Pastukhov, et al., A novel material based on polytrimethylsilylpropyne and hypercrosslinked polystyrene for membrane gas separation and thermopervaporation, Petrol. Chem. 57 (6) (2017) 498–510, https://doi.org/10.1134/S0965544117060032.

[23] A.V. Volkov, E.G. Novitsky, I.L. Borisov, V.P. Vasilevsky, V.V. Volkov, Porous condenser for thermally driven membrane processes: gravity-independent operation, Separ. Purif. Technol. 171 (2016) 191–196, https://doi.org/10.1016/j.seppur.2016.07.038 https://doi.org/10.1016/j.seppur.2016.07.038.

[24] I.L. Borisov, G.S. Golubev, V.P. Vasilevsky, A.V. Volkov, V.V. Volkov, Novel hybrid process for bio-butanol recovery: thermopervaporation with porous condenser assisted by phase separation, J. Membr. Sci. 523 (2017) 291–300, https://doi.org/10.1016/j.memsci.2016.10.009 July 2016 https://doi.org/10.1016/j.memsci.2016.10.009.

[25] A. Kujawska, J. Kujawski, M. Bryjak, W. Kujawski, Removal of volatile organic compounds from aqueous solutions applying thermally driven membrane processes. 1. Thermopervaporation, Chem. Eng. Process-Process Intensification 94 (2015) 62–71, https://doi.org/10.1016/j.cep.2015.02.010 https://doi.org/10.1016/j.cep.2015.02.010.

[26] S. Koter, A. Kujawska, W. Kujawski, Modeling of transport and separation in a thermopervaporation process, J. Membr. Sci. 480 (2015) 129–138, https://doi.org/10.1016/j.memsci.2015.01.044 http://linkinghub.elsevier.com/retrieve/pii/S037673881500071X.

[27] V.A. Kirsh, I.L. Borisov, V.V. Volkov, Hydrodynamics of a thermopervoration flow membrane module with cylindrical spacers, Petrol. Chem. 53 (8) (2013) 578–584, https://doi.org/10.1134/S0965544113080070 http://link.springer.com/10.1134/S0965544113080070.

[28] H. Attia, M.S. Osman, D.J. Johnson, C. Wright, N. Hilal, Modelling of air gap membrane distillation and its application in heavy metals removal, Desalination 424 (2017) 27–36, https://doi.org/10.1016/j.desal.2017.09.027 http://linkinghub.elsevier.com/retrieve/pii/S0011916417314807.

[29] U. Dehesa-Carrasco, C.A. Pérez-Rábago, C.A. Arancibia-Bulnes, Experimental evaluation and modeling of internal temperatures in an air gap membrane distillation unit, Desalination 326 (2013) 47–54, https://doi.org/10.1016/j.desal.2013.07.014 https://doi.org/10.1016/j.desal.2013.07.014.

[30] E. Karbasi, J. Karimi-Sabet, J. Mohammadi-Rovshandeh, M. Ali Moosavian, H. Ahadi, Y. Amini, Experimental and numerical study of air-gap membrane distillation (AGMD): novel AGMD module for Oxygen-18 stable isotope enrichment, Chem. Eng. J. 322 (2017) 667–678, https://doi.org/10.1016/j.cej.2017.03.031 https://doi.org/10.1016/j.cej.2017.03.031.

[31] C. GUIJT, G. MEINDERSMA, T. REITH, A. DEHAAN, Air gap membrane distillation1. Modelling and mass transport properties for hollow fibre membranes, Separ. Purif. Technol. 43 (3) (2005) 233–244, https://doi.org/10.1016/j.seppur.2004.09.015 http://linkinghub.elsevier.com/retrieve/pii/S1383586604003016.

[32] A. Alsaadi, N. Ghaffour, J.D. Li, S. Gray, L. Francis, H. Maab, et al., Modeling of air-gap membrane distillation process: a theoretical and experimental study, J. Membr. Sci. 445 (2013) 53–65, https://doi.org/10.1016/j.memsci.2013.05.049 http://linkinghub.elsevier.com/retrieve/pii/S0376738813004705.

[33] M. Jain, D. Attarde, S.K. Gupta, Removal of thiophene from n-heptane/thiophene mixtures by spiral wound pervaporation module: modelling, validation and influence of operating conditions, J. Membr. Sci. 490 (2015) 328–345, https://doi.org/10.1016/j.memsci.2015.05.004 https://doi.org/10.1016/j.memsci.2015.05.004.

[34] M.T. Ashraf, J.E. Schmidt, J. Kujawa, W. Kujawski, H.A. Arafat, One-dimensional modeling of pervaporation systems using a semi-empirical flux model, Separ. Purif. Technol. 174 (2017) 502–512, https://doi.org/10.1016/j.seppur.2016.10.043 http://linkinghub.elsevier.com/retrieve/pii/S1383586616310796.

[35] M. Jain, D. Attarde, S.K. Gupta, Removal of thiophenes from FCC gasoline by using a hollow fiber pervaporation module: modeling, validation, and influence of module dimensions and flow directions, Chem. Eng. J. 308 (2017) 632–648, https://doi.org/10.1016/j.cej.2016.09.043 https://doi.org/10.1016/j.cej.2016.09.043.

[36] P.M. Schiffmann, Three Step Modelling Approach for the Simulation of Industrial Scale Pervaporation Modules, Ph.D. thesis Technische Universität Bergakademie Freiberg, 2014.

[37] J. Marriott, Detailed Modelling and Optimal Design of Membrane Separation Systems, Ph.D. thesis (2001) http://discovery.ucl.ac.uk/1349890/1/368065.pdf.

[38] Y.A. Çengel, J.M. Cimbala, Fluid Mechanics: Fundamentals and Applications, 3rd. ed., McGraw-Hill, 978-1-259-01122-1, 2014 http://www.uio.no/studier/emner/matnat/math/MEK4450/h11/undervisningsmateriale/modul-5/Pipeflow{_}intro.pdf.

[39] Aspen Technology, Aspen HYSYS V8, 6 (2014).

[40] W.R. Parrish, K.W. Won, M.E. Baltatu, Phase behavior of the triethylenen glycol-water system and dehydration/regeneration design for extremely low dew point requirements, 65th Annual GPA Convention, 1986.

[41] B.E. Poling, J.M. Prausnitz, J.P. O'Connell, fifth ed. ed., The Properties of Gases and Liquids vol. 1, (2001), 0071499997 https://doi.org/10.1016/0070116822 arXiv:arXiv:1011.1669vol. 3.

[42] Engineering ToolBox, Air- Thermal Conductivity, (2009) https://www.engineeringtoolbox.com/air-properties-viscosity-conductivity-heat-capacity-d{_}

[43] DOW, Triethylene Glycol, (2007) http://msdssearch.dow.com/PublishedLiteratureDOWCOM/dh{_}0952/0901b80380952386.pdf?filepath=ethyleneglycol/pdfs/noreg/612-00004.pdf{&}fromPage=GetDoc.

[44] T. Sun2004 Sun, A.S. Teja, Density, viscosity and thermal conductivity of aqueous solutions of propylene glycol, dipropylene glycol, and tripropylene glycol between 290 K and 460 K, J. Chem. Eng. Data 49 (5) (2004) 1311–1317, https://doi.org/10.1021/je049960h.

[45] V. Nafisi, M.B. Hägg, Gas separation properties of ZIF-8/6FDA-durene diamine mixed matrix membrane, Separ. Purif. Technol. 128 (2014) 31–38, https://doi.org/10.1016/j.seppur.2014.03.006 https://doi.org/10.1016/j.seppur.2014.03.006.

[46] H. Zhao, Q. Xie, X. Ding, J. Chen, M. Hua, X. Tan, et al., High performance post-modified polymers of intrinsic microporosity (PIM-1) membranes based on multi-valent metal ions for gas separation, J. Membr. Sci. 514 (2016) 305–312, https://doi.org/10.1016/j.memsci.2016.05.013 https://doi.org/10.1016/j.memsci.2016.05.013.

[47] L. Ansaloni2016a Ansaloni, A. Arif, A.F. Ciftja, H.K. Knuutila, L. Deng, Development of membrane contactors using phase change solvents for CO 2 capture: material compatibility study, Ind. Eng. Chem. Res. 55 (51) (2016) 13102–13113, https://doi.org/10.1021/acs.iecr.6b03901 http://pubs.acs.org/doi/abs/10.1021/acs.iecr.6b03901.

[48] L. Ansaloni, R. Rennemo, H.K. Knuutila, L. Deng, Development of membrane contactors using volatile amine-based absorbents for CO2capture: amine permeation through the membrane, J. Membr. Sci. 537 (April) (2017) 272–282, https://doi.org/10.1016/j.memsci.2017.05.016 https://doi.org/10.1016/j.memsci.2017.05.016.

[49] N.T. Josefsen, Subsea Regeneration of Triethylene Glycol (TEG) for Natural Gas Dehydration, Ph.D. thesis Norwegian University of Science and Technology, 2017.

[50] D. Gorri, M.G. De Angelis, M. Giacinti Baschetti, G.C. Sarti, Water and methanol permeation through short-side-chain perfluorosulphonic acid ionomeric membranes, J. Membr. Sci. 322 (2) (2008) 383–391, https://doi.org/10.1016/j.memsci.2008.05.078.

[51] G.M. Shi, J. Zuo, S.H. Tang, S. Wei, T.S. Chung, Layer-by-layer (LbL) polyelectrolyte membrane with Nexar™ polymer as a polyanion for pervaporation dehydration of ethanol, Separ. Purif. Technol. 140 (2015) 13–22, https://doi.org/10.1016/j.seppur.2014.11.008 https://doi.org/10.1016/j.seppur.2014.11.008.

[52] I.L. Borisov, A.O. Malakhov, V.S. Khotimsky, E.G. Litvinova, E.S. Finkelshtein, N.V. Ushakov, et al., Novel PTMSP-based membranes containing elastomeric fillers: enhanced 1-butanol/water pervaporation selectivity and permeability, J. Membr. Sci. 466 (2014) 322–330, https://doi.org/10.1016/j.memsci.2014.04.037 https://doi.org/10.1016/j.memsci.2014.04.037.

[53] L. Ansaloni2019 Ansaloni, A. Hartono, M. Awais, H.K. Knuutila, L. Deng, CO2 capture using highly viscous amine blends in non-porous membrane contactors, Chem. Eng. J. 359 (2019) 1581–1591, https://doi.org/10.1016/j.cej.2018.11.014 https://doi.org/10.1016/j.cej.2018.11.014.

[54] . DuPont, DuPont ™ Teflon ® AF Amorphous Fluorplastic Resin, (2013) K-26985 7/.

[55] C.A. Scholes, S. Kanehashi, G.W. Stevens, S.E. Kentish, Water permeability and competitive permeation with CO2 and CH4 in perfluorinated polymeric membranes, Separ. Purif. Technol. 147 (2015) 203–209, https://doi.org/10.1016/j.seppur.2015.04.023.

[56] P.R. Resnick, W.H. Buck, Teflon AF amorphous-fluoropolymers, Modern Fluoropolymers, John Wiley & Sons, Ltd, 978-0-471-97055-2, 1997, pp. 397–419 chap. 22.

[57] Engineering ToolBox, Thermal Conductivity of Common Materials and Gases, (2003) https://www.engineeringtoolbox.com/thermal-conductivity-d{_}429.html.

[58] G. Alward, T. Findlay, SI Chemical Data, fifth ed. ed, John Wiley & Sons, Ltd, 0-470-80044-5, 2002.

[59] N. Wang, M.K. Samani, H. Li, L. Dong, Z. Zhang, P. Su, et al., Tailoring the thermal and mechanical properties of graphene film by structural engineering, Small 1801346 (2018) 1–8, https://doi.org/10.1002/smll.201801346.

[60] K. Dalane, M. Hillestad, L. Deng, Subsea natural gas dehydration with membrane processes: simulation and process optimization, Chem. Eng. Res. Des. 142 (2019) 257–267, https://doi.org/10.1016/j.cherd.2018.12.027 https://doi.org/10.1016/j.cherd.2018.12.027.